uc3m | Universidad Carlos III de Madrid

e-Archivo

This is a postprint version of the following published document:

Hernández-Jiménez, F., Sánchez-Prieto, J., Cano-Pleite, E. & Soria-Verdugo, A. (2018). Lateral solids meso-mixing in pseudo-2D fluidized beds by means of TFM simulations. *Powder Technology*, vol. 334, pp. 183–191.

DOI: 10.1016/j.powtec.2018.04.061

© 2018 Elsevier B.V.

This work is licensed under a Creative Commons Attribution-NonCommercial-NoDerivatives 4.0 International License.

Lateral solids meso−mixing in pseudo−2D fluidized beds by means of TFM simulations

F. Hernández-Jiménez [a,*], J. Sánchez-Prieto[b], E. Cano-Pleite[a,c], A. Soria-Verdugo[a]

[a] *Universidad Carlos III de Madrid, Thermal and Fluid Engineering Department, Avda. de la Universidad 30, 28911 Leganés (Madrid), Spain*
[b] *Universidad Internacional de La Rioja (UNIR), Engineering and Technology Faculty. Gran Vía Rey Juan Carlos I, 41. 26002 Logroño, La Rioja, Spain.*
[c] *European Organization for Nuclear Research (CERN), Geneva, Switzerland.*

Abstract

This work studies the solids mixing process in fluidized beds by means of numerical simulations using the two−fluid model (TFM) available in the MFIX code. The numerical results are compared with experiments conducted in a pseudo−2D fluidized bed. The experiments were performed by placing particles of the same diameter and density but of different colour in two vertical layers. To reproduce numerically the experimental results, three phases are defined: one for the gas phase and two for the solid phases, corresponding to the particles of different colours employed in the experiments, to make them separately traceable. To improve the simulation prediction, a friction model that accounts for the effect of the front and rear walls on the continuum solid phases was introduced in the TFM. Mixing times of the

*Corresponding author
Email address: fhjimene@ing.uc3m.es (F. Hernández-Jiménez)

same order of magnitude are obtained from the simulations and the experiments when the mixing process is analysed macroscopically. Furthermore, the simulations are employed to study the solids mixing in the fluidized bed based on a more detailed mixing index. This new mixing index is determined from information of the three phases involved and it is used to predict the mixing behaviours beyond the capabilities of the experimental facility.
Keywords:
Fluidized bed, Solids mixing, Mixing index, TFM, Pseudo−2D, Wall friction

1. Introduction

One of the most important concerns in the study of the fluidization process is the solids mixing [1]. The mixing of particles affects the rates of heat and mass transfer in fluidized beds [2] and its knowledge can be very useful for the design of fuel feeding ports in fluidized bed boilers [3–5]. In many cases, the proper mixing of particles is crucial to ensure a uniform heating, chemical reaction, or drying of the particles and, also, to prevent the formation of hot spots in the bed. The basic mechanism of solids mixing in bubbling fluidized beds is known to be related to bubbles [6]. When a bubble rises through the bed, it carries a wake of particles to the bed surface and there is a permanent displacement or drift of the particles outside the bubble [7]. Axial mixing is induced by bubble rising while lateral mixing is promoted by coalescence and bubble eruption.

The study of the solids mixing in fluidized beds can be performed by analysing the evolution of the bed mixing with time. The most used experimental technique to obtain the mixing evolution consists in marking part of the solids that conformed the packed bed. Then, the variation of concentration of the marked particles in the bed can be visualized if optical access is allowed [8–13] or using indirect methods [14, 15]. Most of the works focussed on visually studying the mixing process are conducted in pseudo-two-dimensional (pseudo-2D) beds, which have been extensively used in the literature to understand the fundamentals of the fludization process, since they allow optical access to the interior of the system [16–24]. Nevertheless, the study of the solids mixing in fluidized beds can be carried out by determining the particles' lateral dispersion coefficient. This is usually done by tracking the motion of a particle or a group of particles inside the bed bulk. The overall dispersion of the tracing particles is measured and fitted to a 1D Fickian-type diffusion equation [3, 25–32]. In particular, this kind of experiments are very helpful to determine the mixing rate of fuel particles inside the fluidised bed reactor [33–35].

Numerical simulations, either using Eulerian−Eulerian two-fluid models (TFM) [36–38], Eulerian−Lagrangian approaches such as discrete element models (DEM) [39, 40], or a combination of both strategies [41], can be a very effective complementary tool for the experiments, to achieve a detailed knowledge of the fluid dynamics of complex gas−solids flows [42, 43]. In the TFM approach, the gas phase and the particles or solid phases are treated as

two inter−penetrating and continuum media in an Eulerian framework. Due to their smaller computational cost compared to DEM, TFM simulations are currently the most suitable strategy for the simulation of the bed when the number of particles involved is high. This allows the simulation of medium and moderately large−sized beds, commonly used in laboratory research and pilot plant testing. In this regard, there are many studies in the literature that employ numerical simulations to study the solids mixing process.

Liu and Chen [4] performed TFM simulations of solids mixing in fluidized beds by adding fictitious tracer particles. These particles were not actually incorporated in the model but were used to track the motion of the solid phase. They analysed the mixing process by means of the lateral dispersion coefficient and they surprisingly found that the dispersion coefficient increases with the bed width, a counterintuitive result. Rhodes *et al.* [6] performed one of the early DEM works to study mixing in fluidized beds. They analysed the simulation results by marking and tracking the DEM particles for both when the bed was already fluidized and for fixed bed conditions. They concluded that mixing time was almost the same regardless the marking procedure. Liu *et al.* [44] carried out DEM simulations to analyse the mixing process, from a qualitative point of view, by injecting individual bubbles. Fang *et al.* [45] and Yang *et al.* [46] analysed the behaviour of an internally circulating fluidized bed by means of DEM simulations. The former study used some preliminary experimental results for the model validation and the latter one incorporated internal tubes in the fluidized bed. Luo *et al.*

[47] qualitatively analysed the differences of lateral and vertical mixing using DEM simulations. Farzaneh *et al.* [48] applied a multigrid Lagrangian technique to study fuel particles motion in two fluidized beds of different width, incorporating also the plenum chamber of the feeding air system. Oke *et al.* [49] performed TFM simulations to study the effect of the model selected for the solids frictional viscosity on the mixing process. They only marked one of the solid phases and attributed the overestimation of the lateral dispersion coefficient to the usage of pure 2D simulations.

The aforementioned studies have used indistinctly DEM and TFM approaches to study different aspects of the mixing process in fluidized beds. Both techniques serve to obtain equivalent information and the main limitation of each approach is the corresponding level of detail of the numerical solution, i.e. particle−scale in the DEM and the so called meso−scale in the TFM. One of the motivations of the present study is to overcome the limitations of the aforementioned numerical studies. On the one hand, the lack of validation with experimental measurements and, on the other hand, to take advantage of the capabilities of the TFM simulations to model medium and moderately large−scale units, and to solve the meso−scale structures of the fluidized bed.

Furthermore, the wall effect in numerical simulations of pseudo−2D fluidized beds has been investigated in several numerical studies using either TFM or CFD−DEM models, demonstrating its relevance [50–57]. Hernández-Jiménez *et al.* [58] developed an empirical model to easily account for the

particle−wall interaction effect in pseudo−2D fluidized beds in a 2D domain, instead of a more computationally demanding 3D domain. The results obtained by Hernández-Jiménez *et al.* [58] showed that the incorporation of the wall−friction term produces a clear improvement of conventional 2D simulations in terms of solids velocity and general bed behaviour. Garcia-Gutierrez *et al.* [59] also applied this friction model to improve the simulation prediction of the motion of fuel particles in pseudo−2D beds.

This work studies the mixing process in fluidized beds by means of numerical simulations. The MFIX−TFM code was selected to carry out the numerical simulations [60, 61] and the numerical results were compared with experiments obtained in a pseudo-2D fluidized bed. The experiments were performed by tracking particles of the same diameter and density but with different colours (black and white) [62]. The same methodology used in the experiments was employed in the TFM simulations. In this case, three phases were defined: one for the gas phase and two for the white and black solid phases to be mixed. The two solid phases were identical, as in the experiments, but they were defined separately in the simulation to make them distinguishable during the post−processing stage. Furthermore, to improve the simulation prediction, a friction model accounting for the effect of the front and rear walls on the continuum solid phase was introduced in the TFM [58]. This model allows for the simulation of the pseudo-2D bed using a standard 2D domain instead of a more computationally demanding 3D domain. The main novelties of the work consist on the validation of the TFM simu-

lation that incorporates the friction term when considering two solid phases and the extra study performed which is allowed by the level of detail of the simulation solution.

2. Experimental set up

The experimental facility employed in this work is a pseudo-2D cold fluidized bed of dimensions 0.3 m x 1 m x 0.01 m (width W, height H, and thickness Z) (Figure 1). More details about the experimental set−up can be found in Sánchez-Prieto *et al.* [62]. The bed was filled with two vertical layers of ballotini glass particles of the same density (2500 kg/m^3), particle size (either 0.4-0.6 mm, 0.6-0.8 mm or 1-1.3 mm) and two different colours (black and white).

[Figure 1 about here.]

The air flow was measured with a set of two flow meters, with ranges of $0 - 200$ L/min and $0 - 500$ L/min providing an accuracy of 1% of full-scale span (FSS). The gas distributor consists of a perforated plate with two rows of 30 holes of 1 mm in diameter arranged in a triangular configuration with 1 cm pitch. The distributor is equipped with a mesh to avoid the falling of particles inside the plenum chamber. This distributor ensures a proper distributor-to-bed pressure drop ratio, to avoid gas maldistribution [63, 64]. The front and rear walls of the bed were made of glass to allow visual access to the bed, and the rear wall was painted in black to increase contrast in the

front image. A summary of the experimental parameters is included in Table 1.

[Table 1 about here.]

A *Nikon* standard digital camera was used to record images of the front wall of the fluidized bed at 60 fps. The spatial resolution of the pictures is 720 x 1280 pixels. A uniform illumination of the front of the bed was guaranteed by the use of two spotlights symmetrically placed at both sides of the bed.

In each experiment, a partition was first inserted at the centre of the bed to divide it into two equal parts. The left part was filled with black painted particles and the right part was filled with white particles. The bed aspect ratio was $H_0/W = 1$ in all the cases. After that, the partition was removed. Finally, the fluidizing air supply was turned on at the desired gas superficial velocity and the bed frontal view was recorded with the digital camera. Three different particle sizes and gas velocities were tested, keeping constant the bed aspect ratio. A summary of the different experiments carried out is shown in Table 2.

[Table 2 about here.]

2.1. Experimental data processing

The most used index to characterize particle mixing is the well−known Lacey index [65], which is defined as:

$$M = \frac{S_0^2 - S^2}{S_0^2 - S_R^2} \tag{1}$$

where S_0^2 is the variance of the completely segregated state, S_R^2 is the variance of the randomly mixed state and S^2 is the variance of the mixture between the completely segregated state and the randomly mixed state. The Lacey index has a zero value for the completely segregated state and increases to unity for the randomly mixed state.

The Lacey index is usually applied to images previously divided into discrete cells and it could be only applied to the experiments of this work provided that it is possible to distinguish between both kind of solid phases and the gas phase (both bubbles and freeboard). As long as the bed rear wall is painted in black, the black solid phase and the gas phase cannot be differentiated in the experimental images. Therefore, a different mixing index, defined in Equation 2, is proposed to characterize the mixing process even when one of the solid phases and the gas are not distinguishable:

$$MI = 1 - \frac{A_{w,i}}{A_{w,max}} \tag{2}$$

where $A_{w,i}$ is the area of the white region of the image i and $A_{w,max}$ is the maximum area of the white region of all the images, which corresponds to a state where the bed has reached the maximum bed expansion. The mixing index, MI, defined in Equation 2 accounts for the variation of the concentration of white region in each image. Each experimental image was

processed to recognize the gray level of each of the pixels in the image (i.e., the concentration of white particles) and binarized [66] to identify the pixels with a high concentration of white particles. Therefore, the rate of disappearance of the white area is estimated. The initial state has the theoretical maximum white area and the final state is reached when no white area is detected in the images. Further details of the processing of the experimental images can be found in Sánchez-Prieto *et al.* [62].

3. Simulation

3.1. Theory

The open−source MFIX−TFM code, developed at US Department of Energy's National Energy Technology Laboratory, was used to conduct the numerical simulations of a 2D bubbling fluidized bed. In the MFIX−TFM code, an Eulerian−Eulerian approach is employed, where both the gas and the solid phases are treated as continuum media. The continuum description of the gas and dense phases is based on the equations of mass and momentum conservation and the granular temperature balance [60, 61].

The numerical simulations account for the particles of different colours by defining two solid phases of identical properties and governing equations. One solid phase is defined for the white solids and the other for the black particles. Therefore, the subscript *s1* is referred to one solid phase, *s2* to the other solid phase and g to the gas phase. Thus, in each of the computational cells, the volume fraction of the three phases must fulfil:

$$\alpha_{s1} + \alpha_{s2} + \alpha_g = 1 \tag{3}$$

The governing equations for the gas and solid phases are the following:

Mass conservation of the gas and solid phases, continuum:

$$\frac{\partial}{\partial t}(\alpha_g \rho_g) + \nabla \cdot (\alpha_g \rho_g \vec{v_g}) = 0 \tag{4}$$

$$\frac{\partial}{\partial t}(\alpha_s \rho_s) + \nabla \cdot (\alpha_s \rho_s \vec{v_s}) = 0 \tag{5}$$

Momentum conservation of the gas phase, continuum:

$$\begin{aligned} \frac{\partial}{\partial t}(\alpha_g \rho_g \vec{v_g}) + \nabla \cdot (\alpha_g \rho_g \vec{v_g} \vec{v_g}) = \\ -\alpha_g \nabla p_g + \nabla \cdot \overline{\overline{\tau_g}} + \alpha_g \rho_g \vec{g} + K_{gs}(\vec{v_s} - \vec{v_g}) \end{aligned} \tag{6}$$

Momentum conservation of the solid phase, continuum:

$$\begin{aligned} \frac{\partial}{\partial t}(\alpha_s \rho_s \vec{v_s}) + \nabla \cdot (\alpha_s \rho_s \vec{v_s} \vec{v_s}) = \\ -\alpha_s \nabla p_g - \nabla p_s + \nabla \cdot \overline{\overline{\tau_s}} + \alpha_s \rho_s \vec{g} - \vec{f}_{fric} + K_{gs}(\vec{v_g} - \vec{v_s}) \end{aligned} \tag{7}$$

where p_i is the pressure and $\overline{\overline{\tau_i}} = \alpha_i \mu_i (\nabla \vec{v_i} + \nabla \vec{v_i}^T) + \alpha_i (\lambda_i - \frac{2}{3}\mu_i) \nabla \cdot \vec{v_i} \overline{\overline{I}}$ is the stress tensor for phase i.

To account for the effect of the front and rear walls of the pseudo$-$2D bed, the extra body force term $\vec{f}_{fric}$ is incorporated in Equation 7, as proposed by Hernández-Jiménez *et al.* [58]. This term can be neglected for the gas phase

as it is expected to have a comparatively minor effect compared to that of the solid phases. The extra body force, per unit of volume of the bed, is expressed as:

$$\vec{f}_{fric} = \frac{2c\vec{v_s}}{Z}\frac{\alpha_s}{\alpha_{s,max}} \tag{8}$$

where c is an empirical coefficient [24], Z is the bed thickness and $\vec{v_s}$ is the solids velocity vector, which is assumed to be equal in both the front and rear walls and equal to the central plane vector velocity in a pseudo$-$2D bed. In Equation 8, the term $\alpha_s/\alpha_{s,max}$ accounts for the effect of the different void fraction of each of the solid phases in a computational cell. Therefore, $\vec{f}_{fric}$ is scaled with the relative amount of solids in each cell. α_s is either α_{s1} or α_{s2}, depending on the solid phase referred to, and $\alpha_{s,max}$ is the maximum solid fraction that can be encountered in a computational cell, which is 0.6 if a void fraction of 0.4 is considered for the dense bed.

Equation 9 is used to calculate the coefficient c in Equation 8, as developed by Hernández-Jiménez *et al.* [58]. Further details about the development and implementation of the term $\vec{f}_{fric}$ can be found in [58].

$$c = 6.2\frac{d_p^2\rho_s g^{1/2}}{Z^{3/2}} + 5.6\cdot 10^{-2}\rho_s Z^{1/2} g^{1/2} \tag{9}$$

Finally, the balance for the granular temperature, Θ, is:

$$\begin{gathered}\frac{3}{2}\left(\frac{\partial}{\partial t}(\rho_s\alpha_s\Theta)+\nabla\cdot(\rho_s\alpha_s\vec{v_s}\Theta)\right)= \\ (-p_s\overline{\overline{I}}+\overline{\overline{\tau_s}}):\nabla\vec{v_s}+\nabla\cdot(k_\Theta\nabla\Theta)-\gamma_\Theta-3K_{gs}\Theta\end{gathered} \tag{10}$$

where $(-p_s\overline{\overline{I}}+\overline{\overline{\tau_s}}):\nabla\vec{v_s}$ is the generation of Θ by the solids stresses, $k_\Theta\nabla\Theta$ is the diffusion of Θ, γ_Θ is the collisional dissipation of Θ and $3K_{gs}\Theta$ is the transfer of random kinetic energy between the solids and the gas. In Equations 6, 7 and 10, K_{gs} is the drag force between the gas and the solid phases. For simplicity, the effect of the front and rear walls on the net production of granular temperature in the bed is not considered here, as it has been proven to have a negligible effect on the velocity profiles [55]. The drag force correlation for the gas−solid interaction used in this work is the one proposed by Gidaspow [37].

A second order accurate scheme was selected to discretise the convective derivatives of the governing equations. The 2D computational domain was meshed using square cells of 5 mm length, as proposed by Li *et al.* [52] and Hernández-Jiménez *et al.* [53] for equivalent systems with bed materials of similar diameters. The distributor was modelled as a uniform velocity inlet and a fixed pressure boundary condition was chosen at the top of the freeboard. The lateral walls of the bed were modelled with a no-slip boundary condition for the gas and solid phases. Each of the solid phases are initially placed at both sides of the bed similarly to the experimental procedure. The

particle diameter used to model the dense phase in the simulations was equal to the average particle diameter in the corresponding experiment and had the same density. The angle of internal friction was set to $\Phi = 30^o$, which is related to the Coulombs coefficient of friction through $\tan\Phi = \mu$. The inter-particle coefficient of restitution was $e_s = 0.9$, the gas density was $\rho_g = 1.2$ kg/m^3 and the gas viscosity was $\mu_g = 1.8 \cdot 10^{-5}$ Pa·s.

4. Results and discussion

4.1. Comparison between experiments and simulation results

Figure 2 shows several selected snapshots of the mixing process for the experiments and both simulation techniques, considering and without considering the friction of the front and rear walls of the bed. The images correspond to the case of $(U_0 - U_{mf}) = 0.66$ m/s and $d_p = 0.6 - 0.8$ mm, which will be considered as the nominal case hereafter, as it makes use of the intermediate particle density and gas excess velocity.

The simulation results are transformed into grayscale images in which only one of the solid phases is represented as white. As in the experiments, the volume fraction of the white particles (α_{s1}) in the computational cells of the right half of the bed progressively decreases as the bed is mixed and the number of cells containing white particles increases. During this process, the white and black particles mix, so that in the fully mixed state the bed is gray, similarly to the experiments. Therefore, using this methodology, the white area recognition in the simulations represents a similar process to that

of the experiments.

As can be observed, a fairly good qualitative agreement is found between the experimental results and the simulations when the frictional term is incorporated to the governing equations. Both black and white particles start to mix at a time around 2 s. At 6 s some remaining clusters of unmixed particles can be distinguished. After approximately 8 s, a randomly mixed state is achieved. In this situation, the mixing reaches a maximum (i.e., MI stabilizes around a value equal to 1). Nevertheless, when analysing the images of the simulation without the friction term, the mixing process is completed at around 4 s, which indicates that the mixing process is much faster than in the experiments.

[Figure 2 about here.]

To quantitatively describe the mixing process, Figure 3 shows the time evolution of the previously defined Mixing Index (MI in Equation 2), for the experimental results and the simulations of the nominal case. The same data processing methodology applied to the experimental images is used in the numerical snapshots to make the comparison as direct as possible. The figure includes also the Lacey's mixing index (Equation 1) calculated on the simulation results with the friction term. The level of detail of the simulation results allows to extract the solids concentration of the two solid phases as well as the gas volume fraction on each computational cell. This permits to calculate the mixing index as originally proposed by Lacey [65]. There-

fore, the blue solid line and the black dash-dot line in Figure 3 represent the evolution of the mixing in the bed but calculated differently (Equations 1 and 2). There could be some scattering in the experimental values of the mixing index during the mixing process, however, this scattering is progressively reduced as the bed approaches the randomly mixed state, obtaining an accurate and repetitive mixing time.

[Figure 3 about here.]

In Figure 3, the differences between the simulations with the wall friction term and without it are clearly noticeable. The slope of the curve of MI in the case without the friction term is much higher than in the simulation that includes the friction term and in the experimental results. Interestingly, the increasing slope of MI in the experiments is quite similar to the simulation results when accounting for the friction term. Also, the time when the randomly mixed state is achieved (i.e., $MI = 1$) in the experiments is also quite similar to the simulations with the friction term, obtaining substantially lower mixing times (time to approach $MI = 1$) when the friction is neglected in the simulations. Besides, when analysing the evolution of the Lacey mixing index (Equation 1), it can be extracted that the results obtained using the white area recognition method (Equation 2) represent almost the same mixing time than the original mixing index developed by Lacey [65]. Despite the curves show little discrepancies in the growing process, the time estimated to reach the randomly mixed state presents a maximum deviation

among the cases studied of ∼1.5 s between Equations 1 and 2. This result corroborates that the simplification used in Equation 2 to obtain the mixing index is valid for the estimation of the time needed for a mixture to achieve a fully randomly mixed state. Further discussion and figures employ the results obtained using Equation 2 to make the comparison with the experiments as direct as possible. Similar evolutions of the mixing curves and similarities with the experimental results are obtained for the rest of the simulation cases with the friction term, but they are not shown for the sake of clarity.

A line corresponding to $MI = 0.95$ is included in Figure 3. This line indicates the time required by the mixture to reach a 95% of the maximum mixing, t_{95}, which is considered as a valid estimation of the mixing time of the fluidized bed [62]. The results obtained for the mixing time, t_{95}, are plotted as a function of the excess gas velocity in Figure 4. The fitting curve included in Figure 4 is obtained from the experimental results, which was linked with the lateral dispersion coefficient reported by Sánchez-Prieto *et al.* [62]. Overall, it can be observed that the inclusion of the friction term in the simulations improves the prediction of the numerical results when compared with the experimental findings. In general, a reasonable deviation of the simulation results including the friction term from the fitting line is obtained in comparison with the experimental results. Discrepancies between the experimental and numerical results seem to increase at low superficial gas velocities for the small and big particle sizes. Besides, the experimental trend is better reproduced by the simulations when accounting for the fric-

tion model. The results of the simulations without the friction term show a systematic under-prediction of the mixing time, especially for the medium and small particle sizes. This is in agreement with Hernández-Jiménez *et al.* [58], who showed that the inclusion of the friction term slows down the overall motion of solids and bubbles. As stated above, bubbles can be considered as the main mechanism of particle mixing in a fluidized bed, thus, a reduction of the motion of solids and the bubble size imply a lower mixing rate.

[Figure 4 about here.]

4.2. Meso mixing index extracted from the simulations

It was observed in the previous section that the simulations, when accounting for the friction of the front and back walls of the bed vessel, are able to reasonably reproduce the experimental findings. Due to the unrestricted availability of data of the simulations, the numerical results can be used to extract more detailed information than the experiments. The MI employed in Figure 3 makes use of the information provided by only one of the solid phases, but the information from the gas phase and the other solid phase is missing. In this situation, variations of the gas volume fraction in the dense bed are neglected. The volume fraction of the two solid phases, as well as the gas volume fraction on each computational cell, can be extracted from the simulations to perform a deeper analysis of the mixing process. Thus, a new Mixing Index (MI^*) can be calculated by comparing the solids volume

fraction of each solid phase on every cell at each time instant. This new Mixing Index, MI^*, (Equation 11) is calculated by computing the number of mixed cells in the bed divided by the total number of cells occupied by solids.

$$MI^* = \frac{N_{mixed}}{N_{total}} \tag{11}$$

where N_{total} is the average total number of cells that are occupied by any of the solid phases when the bed is expanded, and N_{mixed} is the number of cells proved to be properly mixed in each time instant. However, N_{total} is obtained from the time−averaged bed in expanded state, so this value is constant and is related to the time−averaged expanded bed height. In contrast, N_{mixed} changes even for a randomly mixed bed as long as the bed expansion is oscillating due to the passage of bubbles, which produces the oscillation of MI^* around 1, obtaining values higher than 1 for time instants in which the bed expansion is higher than its time−averaged value and lower than 1 when the instant bed expansion is smaller than that value. A cell is considered to be mixed when the difference between the relative volume fraction of the two solid phases is below a threshold value, T:

$$\begin{aligned} &N_{mixed} = 1 \qquad \text{if} \qquad \left|\frac{\alpha_{s1} - \alpha_{s2}}{\alpha_{s1}}\right| < T \\ &N_{mixed} = 0 \qquad \text{otherwise} \end{aligned} \tag{12}$$

Therefore, this new mixing index, MI^*, based on the simulation results

can be considered the mixing state at a meso−scale level, in contrast to the original MI which might correspond to a macro−scale mixing. MI considers only if solids, lightly dependant of the amount, are situated all over the bed. In contrast, MI^* considers the mixing of both solids in the area scrutinized. MI reflects the spread of the tracked solids over the bed while MI^* gives information about the level of presence of the two solids in the region considered. Therefore, MI^* implies the maximum level of detail allowed by the simulations (Equation 3), which in the case of the TFM simulations is the meso−scale level.

Figure 5 shows the mixing curves obtained for different arbitrary values of the threshold T, 0.2, 0.1 and 0.05, for the medium size particles and an excess gas velocity of $U_0 - U_{mf} = 0.66$ m/s and for the simulation results using the friction model. The figure presents only the simulation results that incorporate the friction model because they provide a better prediction of the experimental findings. It can be seen how the mixing time in this case, $t_{95}*$, strongly depends on the value of the threshold employed to consider that a cell is mixed. Reducing the value of this threshold, MI^* (Equation 11) tends to the original MI (Equation 2). In the simulation results, information about the three phases can be extracted and the balance from Equation 3 is fulfilled. Therefore, MI^*, represents a more accurate procedure to discriminate whether a cell is mixed or not, due to the high level of detail of the simulation solution. According to Equation 12, the threshold accounts for different values of relative concentration of solids. The relative concentration

is obtained dividing the difference of concentration of each solid phase by the concentration of one solid phase. Therefore, the lower the threshold, the more similar the concentration of the two solids in a cell is needed to consider this cell mixed. This means that the mixing time changes as the threshold varies since the threshold accounts for the discrimination imposed to decide whether a cell is mixed or not. Ideally, a perfectly mixed state will correspond to cells where the concentration of one solid equals the concentration of the other. However, this criterion is impossible to achieve in a fluidized bed due to its chaotic nature.

[Figure 5 about here.]

Figure 6 shows the mixing time, $t_{95}*$, obtained with the curves resorting from the new definition of the Mixing Index, MI^*, as a function of the excess gas velocity for different values of the threshold used to consider mixing. The figure shows again that different values of the mixing time are found when the selected threshold changes. Besides, certain differences appear when this is compared to the original t_{95}. It can be observed that the new mixing time, $t_{95}*$, is not only dependent on the excess gas velocity, but it seems to be more sensitive to the particle size of the bed material. This decrease with the particle diameter is higher for the smaller particles. Furthermore, a decrease of the new mixing time is typically found with the excess gas velocity.

[Figure 6 about here.]

4.3. Analysis of mixing indexes

Once the simulations of the mixing process in fluidized beds including the friction term were validated with experimental data, the results obtained from the simulations were employed to discuss the results obtained for the mixing time from the different definitions of mixing indexes analysed. No experimental data was included in the comparison since the calculation of the Lacey mixing index (Equation 1) and the meso−scale mixing index MI^* (Equation 11) requires the solids and gas phases to be distinguishable.

The temporal evolution of the different mixing indexes obtained from the simulations considering the friction term for the medium size particle and excess gas velocity, (i.e., $d_p = 0.6 - 0.8$ mm and $U_0 - U_{mf} = 0.66$ m/s), are shown in Figure 7. In the case of the meso−scale mixing index, only the evolution of MI^* for a threshold of 0.2 is included in the comparison. As stated above, the evolution of the Lacey mixing index (Equation 1) and the mixing index defined in Equation 2 is similar, obtaining similar values for the mixing time in both cases. In contrast, the meso−scale mixing index MI^* (Equation 11) lead to slightly larger mixing times, since the definition of a randomly mixed fluidized bed using MI^* is more restrictive due to the use of information of both solid phases in each cell of the bed.

[Figure 7 about here.]

The comparison of the mixing times obtained from the different definition of mixing indexes applied to the results of the simulations considering the

friction term is extended to all the particle sizes and excess gas velocities in Figure 8. The mixing time obtained from the definition of the macro−scale mixing indexes, i.e., the Lacey mixing index (Equation 1) and MI (Equation 2), are very similar, whereas the application of the meso−scale mixing index MI^* (Equation 11) resulted in longer mixing times for all the cases analysed, due to the more restrictive definition of the randomly mixed state using MI^*. In view of the mixing times obtained, shown in Figure 8, the mixing index MI (Equation 2) can be said to lead to accurate values of the mixing time, even though this mixing index requires information of only one of the solid phases. In fact, the results obtained for the mixing time for the definition of MI (Equation 2) are between those obtained from the Lacey mixing index (Equation 1) and from the meso−scale mixing index (Equation 11). Therefore, the easily applicable definition of mixing time MI given by Equation 2 can be employed to describe the mixing process in pseudo-2D fluidized beds even when only one of the solid phases can be distinguishable from the gas phase.

[Figure 8 about here.]

5. Conclusions

This work studied the different mixing mechanisms in fluidized beds by means of numerical simulations. The numerical results were compared with the experimental evidence obtained in a pseudo−2D fluidized bed that allows optical access to the interior of the system through the frontal glass wall of

the bed vessel. The prediction of the numerical simulations was improved by incorporating a friction model that accounts for the effect of the front and rear walls in the 2D simulated bed without the need to incorporate such walls in a 3D simulation domain. The simulations were employed to analyse the mixing in the fluidized bed in more detail, as they provide information about the two solid phases. The new mixing time defined was found to decrease with the excess gas velocities with different decreasing rates depending on the particle size. The mixing index proposed in this work (Equation 2) requires less information about the solid phases than the Lacey and the meso−mixing indexes. However, the mixing times obtained from MI^* are similar to those extracted from the Lacey and meso−mixing indexes for all the cases studied.

Acknowledgments

The authors gratefully acknowledge the financial support provided by Fundación Iberdrola under the "Programa de Ayudas a la Investigación en Energía y Medioambiente 2016".

Notation

$A_{w,max}$	Area of the white region of the expanded bed (pixels^2)
$A_{w,i}$	Area of the white region of the image i (pixels^2)
c	Particle-wall interaction coefficient, (kg/(m^{2}s))
d_p	Particle diameter (mm)
e_s	Restitution coefficient (-)

$\vec{f}_{fric}$	Friction force due the the frontal and rear walls (N)
$\vec{g}$	Gravity (m/s^2)
H	Bed height (m)
H_0	Static bed height (m)
H_0/W	Bed aspect ratio (-)
$\overline{\overline{I}}$	Unity matrix (-)
K_{gs}	Drag force between gas and solids, (kg/(m^{3}s))
k_Θ	Diffusion coefficient for granular energy, (kg/(m s))
M	Lacey mixing index (-)
MI	Mixing index (-)
MI^*	Modified mixing index (-)
m_p	Mass of particles in the bed (kg)
N_{mixed}	Number of computational cells mixed (-)
N_{total}	Total number of computational occupied by solids (-)
p_g	Gas pressure (Pa)
p_s	Solids pressure (Pa)
S^2	Variance of the mixture (-)
S_0^2	Variance of the completely segregated state (-)
S_R^2	Variance of the randomly mixed state (-)
T	threshold to discriminate a mixed cell (-)
t	Time (s)
t_{95}	Time at which $MI = 0.95$ (s)
$t_{95}*$	Time at which $MI^* = 0.95$ (s)

U_0	Air superficial velocity (m/s)
U_{mf}	Minimum fluidization velocity (m/s)
$\vec{v_g}$	Gas velocity (m/s)
$\vec{v_s}$	Solids velocity (m/s)
x	Spatial coordinate (m)
W	Bed width (m)
Z	Bed thickness (m)

Greek letters

α_g	Gas concentration (-)
α_s	Solid concentration (-)
$\alpha_{s,max}$	Maximum solid concentration (-)
γ_Θ	collisional dissipation of (m^2/s^2)
μ_g	Gas viscosity, (Pa s)
Φ	Angle of internal friction (deg)
ρ_g	Gas density (kg/m^3)
ρ_s	Particle density (kg/m^3)
τ	Stress tensor (Pa)
Θ	Granular temperature (m^2/s^2)

References

[1] D. Kunii, O. Levenspiel, *Fluidization engineering*, (1991) Butterworth-Heinemann, Stoneham, UK, 2nd ed.

[2] G.A. Bokkers, M. van Sint Annaland, J.A.M. Kuipers, Mixing and segregation in a bidisperse gas-solid fluidized bed: a numerical and experimental study, *Powder Technol.* 140 (2004) 176-186.

[3] F. Niklasson, H. Thunman, F. Johnsson, B. Leckner, Estimation of solids mixing in a fluidized-bed combustor, *Ind. Eng. Chem. Res.* 41 (2002) 4663-4673.

[4] D. Liu and X. Chen, Lateral solids dispersion coefficient in large-scale fluidized beds, *Combust. Flame* 157 (2010) 2116-2124.

[5] L.M. Garcia-Gutierrez, A. Soria-Verdugo, U. Ruiz-Rivas, Optimization of the feeding ports location in a fluidized bed combustor based on Monte Carlo simulations of fuel particles motion, *Fuel* 141 (2015) 82-92.

[6] M.J. Rhodes, X.S. Wang, M. Nguyen, P. Stewart, K. Liffman, Study of mixing in gas-fluidized beds using a DEM model, *Chem. Eng. Sci.* 56 (2001) 2859-2866.

[7] I. Eames, M.A. Gilbertson, Mixing and drift in gas-fluidised beds, *Powder Technol.* 154 (2005) 185-193.

[8] A.S. Hull, Z. Chen, P.K. Agarwal, Influence of horizontal tube banks on the behavior of bubbling fluidized beds: 2. Mixing of solids, *Powder Technol.* 111 (2000) 192-199.

[9] Y. Zhang, B. Jin, W. Zhong, Experiment on particle mixing in flat-bottom spout-fluid bed, *Chem. Eng. Process.* 48 (2009) 126-134.

[10] S. Gorji-Kandi, S.M. Alavi-Amleshi, N. Mostoufi, A solids mixing rate correlation for small scale fluidized beds, *Particuology* 21 (2015) 55-64.

[11] I. Julián, J. Herguido, M. Menéndez, Particle mixing in a two-section two-zone fluidized bed reactor. experimental technique and counter-current back-mixing model validation, *Ind. Eng. Chem. Res.* 52 (2013) 13587-13596.

[12] I. Julián, J. Herguido, M. Menéndez, Experimental and simulated solids mixing and bubbling behavior in a scaled two-section two-zone fluidized bed reactor, *Chem. Eng. Sci.* 143 (2016) 240-255.

[13] E. Cano-Pleite, F. Hernández-Jiménez, A. Acosta-Iborra, T. Tsuji, C.R. Müller, Segregation of equal-sized particles of different densities in a vertically vibrated fluidized bed, *Powder Technol.*, 316, 2017, 101-110.

[14] E. Sette, D. Pallars, F. Johnsson, Experimental evaluation of lateral mixing of bulk solids in a fluid-dynamically down-scaled bubbling fluidized bed, *Powder Technol.*, 263, 2014, 74-80.

[15] E. Sette, D. Pallars, F. Johnsson, Influence of bulk solids cross-flow on lateral mixing of fuel in dual fluidized beds, *Fuel Process. Technol.*, 140, 2015, 245-251.

[16] L. Shen, F. Johnsson, B. Leckner, Digital image analysis of hydrodynamics two-dimensional bubbling fluidized beds, *Chem. Eng. Sci.* 59 (2004) 2607-2617.

[17] C.R. Müller, J.F. Davidson, J.S. Dennis, A.N. Hayhurst, A study of the motion and eruption of a bubble at the surface of a two-dimensional fluidized bed using particle image velocimetry (PIV), *Ind. Eng. Chem. Res.* 46 (2007) 1642-1652.

[18] J.A. Laverman, I. Roghair, M. van Sint Annaland, J.A.M. Kuipers, Investigation into the hydrodynamics of gas-solid fluidized beds using particle image velocimetry coupled with digital image analysis, *Can. J. Chem. Eng.* 86 (2008) 523-535.

[19] A. Busciglio, G. Vella, G. Micale, L. Rizzuti, Analysis of the bubbling behaviour of 2D gas solid fluidized beds: Part I. Digital image analysis technique, *Chem. Eng. J.* 140 (2008) 398-413.

[20] S. Sánchez-Delgado, C. Marugán-Cruz, A. Soria-Verdugo, D. Santana, Estimation and experimental validation of the circulation time in a 2D gas-solid fluidized bed, *Powder Technol.* 150 (2013) 1-8.

[21] A. Soria-Verdugo, L.M. Garcia-Gutierrez, S. Sánchez-Delgado, U. Ruiz-Rivas, Circulation of an object inmersed in a bubbling fluidized bed, *Chem. Eng. Sci.* 66 (2011) 78-87.

[22] A. Soria-Verdugo, L.M. Garcia-Gutierrez, N. García-Hernando, U. Ruiz-Rivas, Bouyancy effects on objects moving in a fluidized bed, *Chem. Eng. Sci.* 66 (2011) 2833-2841.

[23] F. Hernández-Jiménez, J.R. Third, A. Acosta-Iborra, C.R. Müller, Comparison of bubble eruption models with two-fluid simulations in a 2D gas-fluidized bed, *Chem. Eng. J.* 171 (2011) 328-339.

[24] F. Hernández-Jiménez, J. Sánchez-Prieto, A. Soria-Verdugo, A. Acosta-Iborra, Experimental quantification of particle-wall frictional forces in pseudo-2D gas fluidised beds, *Chem. Eng. Sci.* 102 (2013) 257-267.

[25] D. Bellgardt, M. Schoessler, J. Werther, Lateral non-uniformities of solids and gas concentrations in fluidized bed reactors, *AIChE Annual Meeting* 1986.

[26] V.A. Borodulya, Y.G. Epanov, Y.S. Teplitskii, Horizontal particle mixing in a free fluidized bed, *J. Eng. Phys. Thermophys.* 42 (1982) 528-533.

[27] L. Glicksman, E. Carr, P. Noymer, Particle injection and mixing experiments in a one-quarter scale model bubbling fluidized bed, *Powder Technol.* 180 (2008) 284-288.

[28] L. Shen and M. Zhang, Effect of particle size on solids mixing in bubbling fluidized beds, *Powder Technol.* 97 (1998) 170-177.

[29] Y.F. Shi, L.T. Fan, Lateral mixing of solids in batch gas-solids fluidized beds, *Ind. Eng. Chem. Process Des. Dev.* 23 (1982) 337-341.

[30] D. Bellgardt and J. Werther, A novel method for the investigation of particle mixing in gas-solid systems, *Powder Technol.* 48 (1986) 173-180.

[31] N. Mostoufi and J. Chaouki, On the axial movement of solids in gas-solid fluidized beds, *Trans IChemE* 78 (2000) 911-920.

[32] J. Olsson, D. Pallares, F. Johnsson, Lateral fuel dispersion in a large-scale bubbling fluidized bed, *Chem. Eng. Sci.* 74 (2012) 148-159.

[33] E. Sette, D. Pallarès, F. Johnsson, Experimental quantification of lateral mixing of fuels in fluid-dynamically down-scaled bubbling fluidized beds, *Appl. Energy* 136 (2014) 671-681.

[34] E. Sette, D. Pallars, F. Johnsson, F. Ahrentorp, C. Johansson, Magnetic tracer-particle tracking in a fluid dynamically down-scaled bubbling fluidized bed, *Fuel Process. Technol.* 138 (2015) 368-377.

[35] E. Sette, T. Berdugo Vilches, D. Pallarès, F. Johnsson, Measuring fuel mixing under industrial fluidized-bed conditions - A camera-probe based fuel tracking system, *App. Energy* 163 (2016) 304-312.

[36] Kuipers, J.A.M., Van Duin, K.J., Van Beckum, F.P.H., Van Swaaij, W.P.M., A numerical model of gas-fluidized beds *Chem. Eng. Sci.*, 47 (1992), 1913-1924.

[37] Gidaspow, D., Multiphase flow and Fluidization: Continuum and kinetic theory descriptions; Academic Press: San Diego, CA. 1994.

[38] van Wachem, B.G.M., Almstedt, A.E., Methods for multiphase computational fluid dynamics. *Chem. Eng. J.*, 96 (2003), 81-98.

[39] Deen, N.G., van Sint Annaland, M., van der Hoef, M.A., Kuipers, J.A.M., Review of discrete particle modelling of fluidized beds. *Chem. Eng. Sci.*, 62 (2007), pp. 28-44

[40] Müller, C.R., Holland, D.J., Sederman, A.J., Scott, S.A., Dennis, J.S., Gladden, L.F., Granular temperature: Comparison of Magnetic Resonance measurements with Discrete Element Model simulations. *Powder Technol.*, 203 (2008), 241-253.

[41] F.Hernández-Jiménez, L.M. García-Gutiérrez, A. Soria-Verdugo, A. Acosta-Iborra, Fully coupled TFM-DEM simulations to study the motion of fuel particles in a fluidized bed, *Chem. Eng. Sci.* 134 (2015) 57-66.

[42] Grace, J.R., Taghipour, F., Verification and validation of CFD models and dynamic similarity for fluidized beds. *Powder Technol.*, 139 (2004), 99-110.

[43] Grace, J.R. and Li., T., Complementarity of CFD, experimentation and reactor models for solving challenging fluidization problems. *Particuology*, 8 (2010), 498-500.

[44] D. Liu, S. Xiao, X. Chen, C. Bu, Investigation of solid mixing mechanisms in a bubbling fluidized bed using a DEM-CFD approach, *Asia-Pac. J. Chem. Eng.* 7(2) (2012) S237-S244.

[45] M. Fang, K. Luo, S. Yang, K. Zhang, J. Fan, Computational fluid dynamics discrete element method investigation of solid mixing characteristics in an internally circulating fluidized bed, *Ind. Eng. Chem. Res.* 52 (2013) 7556-7568.

[46] S. Yang, K. Luo, M. Fang, J. Fan, Influence of tube configuration on the gas-solid hydrodynamics of an internally circulating fluidized bed: a discrete element study, *Chem. Eng. J.* 239 (2014) 158-170.

[47] K. Luo, F. Wu, S. Yang, J. Fan, CFD-DEM study of mixing and dispersion behaviors of solid phase in a bubbling fluidized bed, *Powder Technol.* 274 (2015) 482-493.

[48] M. Farzaneh, S. Sasic, A.E. Almstedt, F. Johnsson, D. Pallarès, A study of fuel particle movement in fluidized beds, *Ind. Eng. Chem. Res.* 52 (2013) 5791-5805.

[49] O. Oke, P. Lettieri, P. Salatino, R. Solimene, L. Mazzei, Numerical

simulations of lateral solid mixing in gas-fluidized beds, *Chem. Eng. Sci.* 120 (2014) 117-129.

[50] T. Kawaguchi, T. Tanaka, Y. Tsuji, Numerical simulation of two-dimensional fluidized beds using the discrete element method (comparison between the two- and three-dimensional models), *Powder Technol*, 96, 1998, 129-138.

[51] Y.Q. Feng, A.B. Yu, Effect of bed thickness on the segregation behavior of particle mixtures in a gas fluidized bed *Ind. Eng. Chem. Res.*, 49 (2010), pp. 34593468

[52] T. Li, J.R. Grace, X. Bi Study of wall boundary condition in numerical simulations of bubbling fluidized beds *Powder Technol.*, 203 (2010), pp. 447457

[53] F. Hernández-Jiménez, S. Sánchez-Delgado, A. Gómez-García, A. Acosta-Iborra, Comparison between two-fluid model simulations and particle image analysis & velocimetry (PIV) results for a two-dimensional gas-solid fluidized bed, *Chem. Eng. Sci.* 66 (2011) 3753-3772.

[54] T. Li, P. Gopalakrishnan, R. Garg, M. Shahnam CFD-DEM study of effect of bed thickness for bubbling fluidized beds. *Particuology*, 10 (2012), pp. 532541

[55] Li, T., Zhang Y., A new model for two-dimensional numerical simulation of pseudo-2D gas-solids fluidized beds. *Chem. Eng. Sci.*, 102 (2013), 256-256.

[56] F. Hernández-Jiménez, T. Li, E. Cano-Pleite, W. Rogers, A. Acosta-Iborra, Characterization of the particle-wall frictional forces in pseudo-2D fluidized beds using DEM, *Chem. Eng. Sci.*, 116 (2014), pp. 136143

[57] T. Li, Y. Zhang, F. Hernández-Jiménez, Investigation of particlewall interaction in a pseudo-2D fluidized bed using CFD-DEM simulations, *Particuology*, 25 (2016), 10-22.

[58] F. Hernández-Jiménez, J. Snchez-Prieto, E. Cano-Pleite, L.M. Garcia-Gutierrez, A. Acosta-Iborra, Development of an empirical wall-friction model for 2D simulations of pseudo-2D bubbling fluidized beds, *Advanced Powder Technology*, 27, 2, (2016), 521-530.

[59] L.M. Garcia-Gutierrez, F. Hernndez-Jimnez, E. Cano-Pleite, A. Soria-Verdugo, Improvement of the simulation of fuel particles motion in a fluidized bed by considering wall friction, *Chem. Eng. J.* 321 (2017), 175-183.

[60] Syamlal, M., Rogers, W., O'Brien, T.J., MFIX Documentation: Theory guide, U.S. department of Energy (DOE), Morgantown Energy Technology Center, Morgantown, West Virginia, 1993.

[61] Benyahia, S., Syamlal, M., O'Brien, T.J., Summary of MFIX equations 2005-4, 2007.

[62] J. Sánchez-Prieto, F. Hernández-Jiménez, L.M. Garcia-Gutierrez, A. Soria-Verdugo, Experimental study on the characteristic mixing time of solids and its link with the lateral dispersion coefficient in bubbling fluidized beds, *Chemical Engineering Journal*, 307, 2017, 113-121.

[63] S.B.R. Karri, J. Werther, Gas distributor and plenum design in fluidized beds. In: W.C. Yang, *Handbook of fluidization and fluid-particle systems*. Marcel Dekker Inc., New York, (2003) 164-179.

[64] J. Sánchez-Prieto, A. Soria-Verdugo, J.V. Briongos, D. Santana, The effect of temperature on the distributor design in bubbling fluidized beds, *Powder Technol.* 261 (2014) 176-184.

[65] P.M.C. Lacey, Developments in the theory of particle mixing, *J. Appl. Chem.* 4 (1954) 257-268.

[66] Otsu, N., A threshold selection method from gray-level histograms, *IEEE Transactions on Systems Man and Cybernetic*s 9 (1979) 62-66.

List of Figures

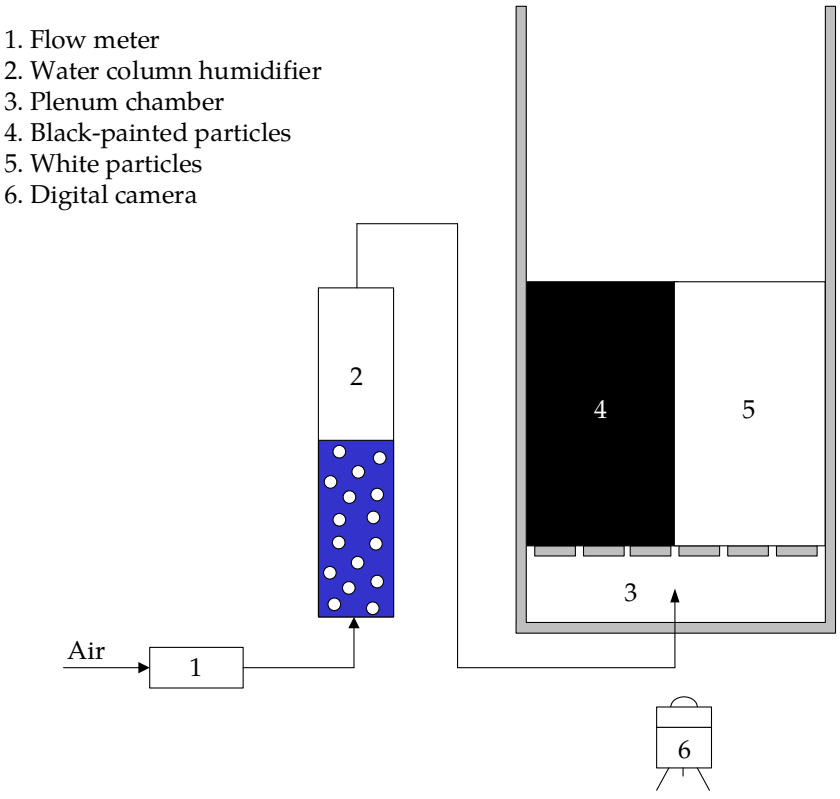

Figure 1: Schematic diagram of the experimental setup.

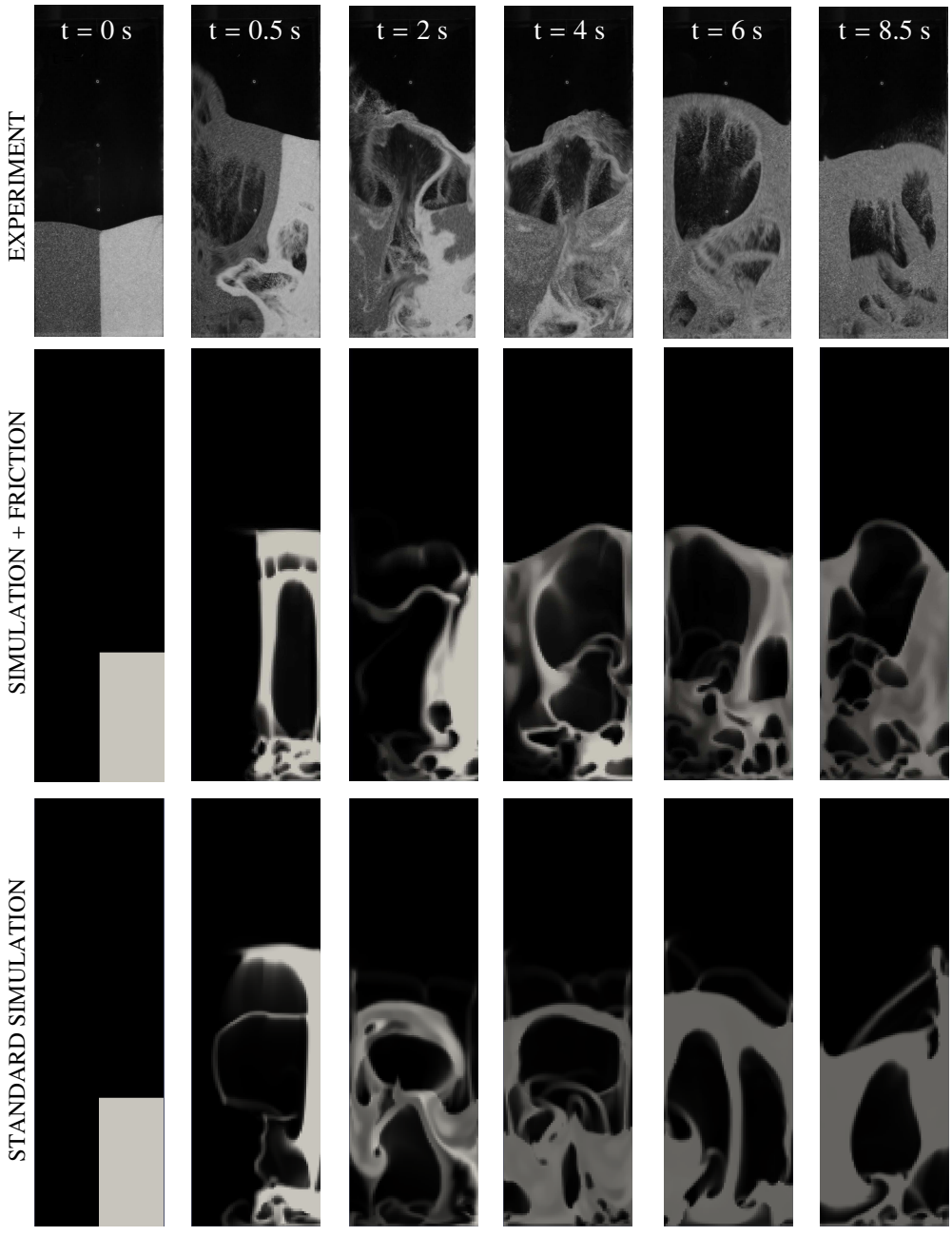

Figure 2: Example of a mixing process ($(U_0 - U_{mf}) = 0.66$ m/s, $d_p = 0.6 - 0.8$ mm).

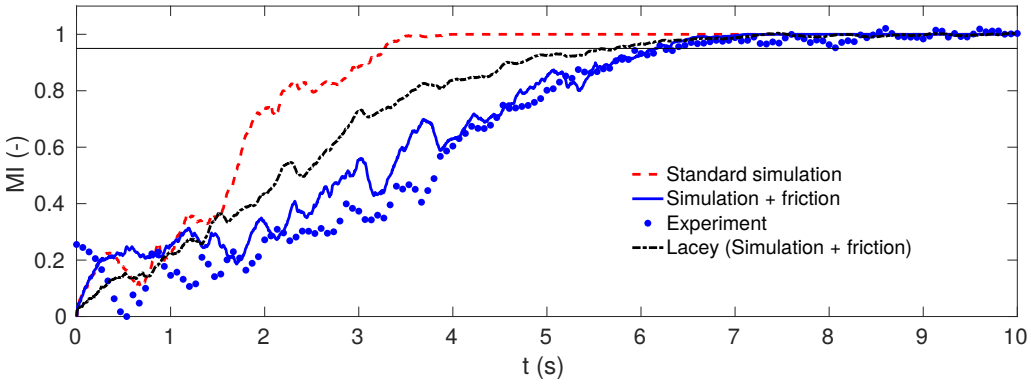

Figure 3: Mixing index as a function of time ($(U_0 - U_{mf}) = 0.66$ m/s, $d_p = 0.6 - 0.8$ mm).

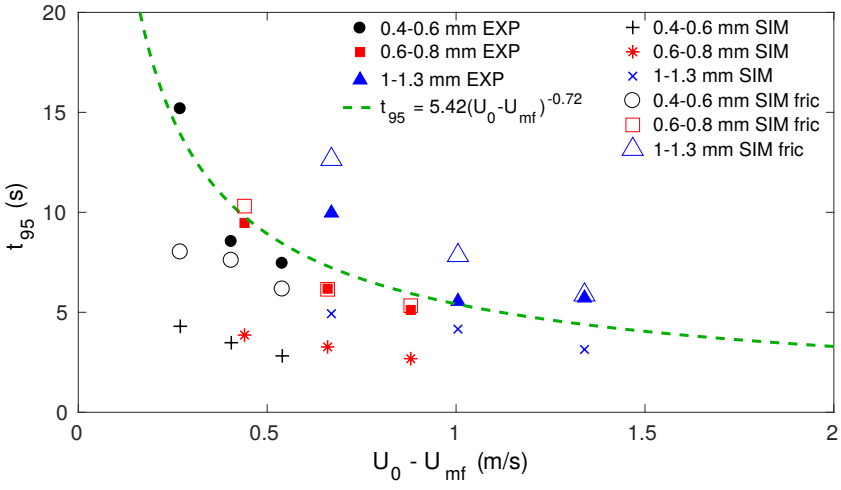

Figure 4: Mixing time, t_{95}, as a function of the excess gas velocity, $U_0 - U_{mf}$.

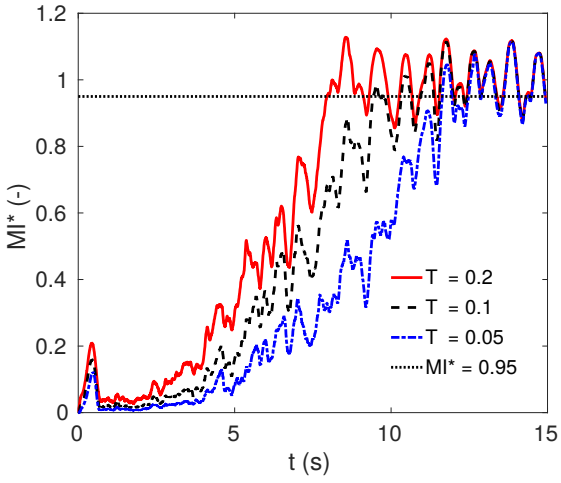

Figure 5: Time evolution of MI^* (Equation 11) for the simulation results with the friction term. d_p = 0.6-0.8 mm. $U_0 - U_{mf}$ = 0.66 m/s

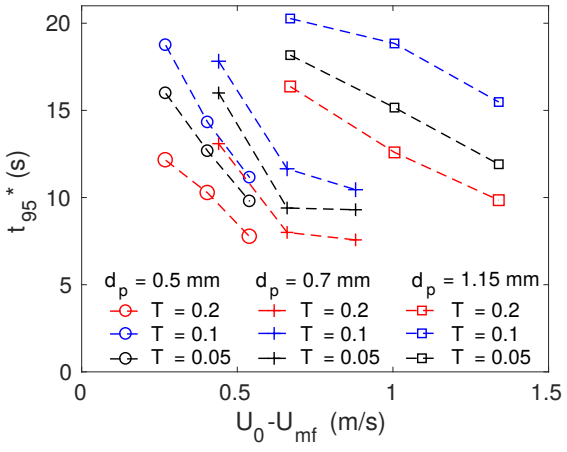

Figure 6: Mixing time, $t_{95}*$, as a function of the excess gas velocity, $U_0 - U_{mf}$, for the simulation results with the friction term.

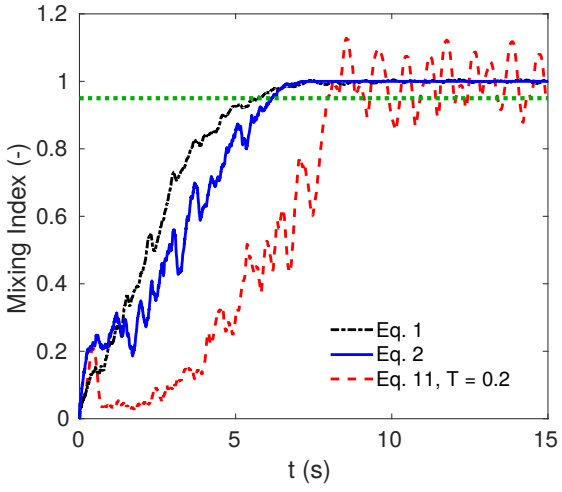

Figure 7: Time evolution of the different mixing indexes obtained from the simulations considering the friction term for $d_p = 0.6 - 0.8$ mm and $U_0 - U_{mf} = 0.66$ m/s.

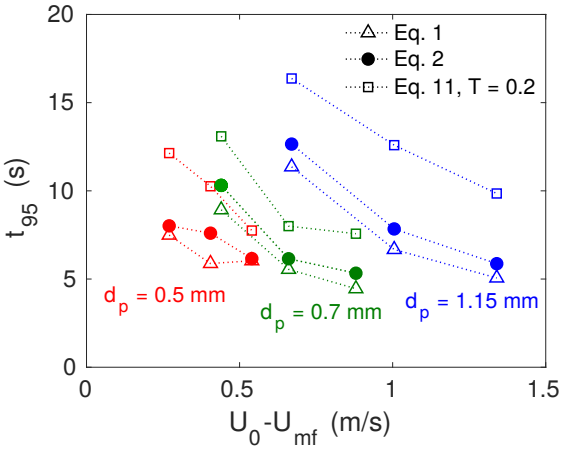

Figure 8: Mixing times obtained from the mixing indexes defined in Equations 1, 2 and 11, for the simulation considering the friction term.

List of Tables

Table 1: Summary of experimental conditions.

Parameter		Value
Bed height, H(m)		1
Bed width, W(m)		0.3
Bed thickness, Z(m)		0.01
Aspect ratio, H_0/W (-)		1
Particles density, ρ_s(kg/m^3)		2500
Small particles	d_p(mm)	0.4-0.6
	U_{mf}(m/s)	0.27
Medium particles	d_p(mm)	0.6-0.8
	U_{mf}(m/s)	0.44
Big particles	d_p(mm)	1-1.3
	U_{mf}(m/s)	0.67

Table 2: Summary of experiments.

Particle size (mm)	U_{mf} (m/s)	$U_0 - U_{mf}$(m/s)		
		$U_0 = 2U_{mf}$	$U_0 = 2.5U_{mf}$	$U_0 = 3U_{mf}$
1-1.3	0.67	0.67	1.005	1.34
0.6-0.8	0.44	0.44	0.66	0.88
0.4-0.6	0.27	0.27	0.405	0.54